

Quasinormal modes, thermodynamics and shadow of black holes in Hu-Sawicki $f(R)$ gravity theory

Ronit Karmakar * and Umananda Dev Goswami †

Department of Physics, Dibrugarh University, Dibrugarh 786004, Assam, India

We derive novel black hole solutions in a modified gravity theory, namely the Hu-Sawicki model of $f(R)$ gravity. After obtaining the black hole solution, we study the horizon radius of the black hole from the metric and then analyse the dependence of the model parameters on the horizon. We then use the 6th order WKB method to study the quasinormal modes of oscillations (QNMs) of the black hole perturbed by a scalar field. The dependence of the amplitude and damping part of the QNMs are analysed with respect to variations in model parameters and the error associated with the QNMs are also computed. After that we study some thermodynamic properties associated with the black hole such as its thermodynamic temperature as well as greybody factors. It is found that the black hole has the possibility of showcasing negative temperatures and is thermodynamically unstable for feasible values of model parameters. Then we analyse the geodesics and derive the photon sphere radius as well as the shadow radius of the black hole. The photon radius is independent of the model parameters while shadow radius showed fair amount of dependence on the model parameters. We tried to constrain the parameters with the help of Keck and VLTI observational data and obtained some bounds on m and c_2 parameters.

Keywords: Hu-Sawicki gravity; Black holes; Quasinormal modes; Thermodynamics; Shadow

I. INTRODUCTION

General relativity (GR) has undoubtedly been successful in accounting for observational results in the solar system and beyond [1, 2]. GR theory predicts with great accuracy the precession of the perihelion of planet Mercury [1, 3] and bending of light due to gravitational field [4] in the local as well as distant observations. GR has predicted the existence of black holes and gravitational waves (GWs) which has been recently experimentally verified by the LIGO-Virgo collaboration [5–9]. The recent direct images of the black hole shadows published by the Event Horizon Telescope (EHT) group [10–15] also back GR in terms of experimental verification of the theory. In spite of these successes, GR fails to address recent observations like the accelerated expansion of the Universe [16–18]. Indeed, it does not provide any insights regarding the dark components of the Universe [19, 20]. Thus, to overcome these issues, physicists worked on modified theories of gravity, the most common among them includes the Λ CDM [21] model, $f(R)$ gravity theory [22–25], $f(R, T)$ gravity theory [26], $f(Q)$ gravity theory [27–30] and so on (see [31]). These theories can compensate for the effects of dark components [32], explain galactic rotation curves [33], accelerated expansion of the Universe [34, 35] and are well constrained by modern observations. Rastall gravity proposed in 1972 is arguably a unique modified theory of gravity which does not follow from an established Lagrangian formalism [36]. It advocates the violation of conservation of energy-momentum tensor $T_{\mu\nu}$ and equates it to the derivative of the Ricci scalar R . In recent times, a number of $f(R)$ gravity models have been proposed, some of them include Starobinsky [37], Hu-Sawicki [38], Sujikawa [40] and other two models mentioned in Refs. [39, 41] to name a few. These models have been extensively studied in the literature regarding various aspects like their cosmological and astrophysical implications [33, 42–44], dynamical system analysis [45, 46], early Universe mysteries [47] and so on. Similarly, $f(Q)$ gravity has also attracted a lot of attention in the recent times and many cosmological studies have been carried out in this theory, for instance see Refs. [46, 48–50] and references therein.

The first vacuum solution of the Einstein field equations leading to a black hole was given by Schwarzschild in 1916 [51]. Since then, a number of black hole solutions have been proposed from time to time in various frameworks of gravity. Black holes are often studied with an engulfing field around them. These fields may include quintessence fluid [52–55], matter in the form of dust, radiation [56], plasma [57], dark matter halo [58] and so on. These surrounding fields have impacts on various thermodynamic properties, quasinormal modes (QNMs), shadow radius etc. of black holes and have been extensively studied in the literature. In a recent paper [53], GUP-improved Schwarzschild-type solution, its thermodynamic properties and quasinormal modes have been studied. In another work [59], a Schwarzschild-type black hole in Bumblebee gravity has been considered and its thermodynamics and shadow have been studied.

Black hole solutions have been derived in the framework of $f(R)$ gravity in many recent papers. In Ref. [39], Saffari and Rahvar derived novel black hole solutions in the $f(R)$ framework and also proposed a novel $f(R)$ form that is feasible in both

* Email: ronit.karmakar622@gmail.com

† Email: umananda@dibru.ac.in

local and galactic scales. In Ref. [60], the authors derived black hole solutions in various $f(R)$ models. In a recent work [61], novel black hole solutions were derived in various $f(R)$ models and the authors studied topological and thermodynamic properties of the solutions obtained. Motivated by these ongoing researches, we derive novel black hole solutions in Hu-Sawicki gravity. Here, we intend to study various properties relating to the black hole solutions obtained. Our solution is unique in the sense that the black hole solution for the Hu-Sawicki model of $f(R)$ gravity has not been worked out before to the best of our knowledge and thus we are motivated to study its properties including QNMs, thermodynamics as well as shadow radius and greybody factors.

Further, the black hole's shadow also has gained a fair amount of attention, credits to the recently released data and images of the black holes at the center of M87 galaxy and Sgr A. This has opened up a new window to constrain various theories of gravity and parameter values as well. Recently in Ref. [62], different parameters of modified theories of gravity have been constrained using modern shadow radius data. Another work [63] constraints regular black hole parameters with shadow data of the EHT. Recent works regarding black hole shadows have gained momentum as shadow provides interesting new insights and data to constrain black hole physics [64–72].

QNMs of oscillations of a perturbed black hole hold promise of constraining physics at the extreme regimes of black holes. The QNMs are basically complex frequencies linked to GWs produced when a black hole is perturbed by some external means. There has been an upsurge of research regarding various aspects of QNMs, new techniques of computing QNMs, their relationships with shadow data and so on. The WKB method of computing QNMs is the most widely used technique, though many spectral and analytical techniques are often used in combination. There has been a wide range of applications of QNMs in understanding various phenomena such as testing the No-Hair theorem [73] and constraining theories of modified gravity [74]. QNMs can also be used to study the stability of background spacetime when it is acted upon by a minute perturbation [75]. The relation between shadow radius and QNMs has been dealt with in Ref. [72]. QNMs and Hawking radiation sparsity for GUP-corrected black holes with topological defects have been studied in Ref. [76]. A brief account of various methods employed in recent times to compute the QNMs can be found in the Refs. [76–80].

Black hole thermodynamics has gained momentum and attracted a lot of attention following the path-breaking work of Bekenstein and Hawking [81–83]. Their idea led to the development of four laws of black hole thermodynamics. Recently a number of research works have been carried out in this field. Schwarzschild black holes with quantum corrections have been investigated for scattering and absorption cross-section [84]. In Ref. [85], the authors studied absorption and scattering by a black hole with a global monopole in $f(R)$ gravity. Recently, thermodynamic properties of extended GUP-corrected black holes has been carried out in Ref. [86]. Thermodynamics of static dilaton black holes have been studied in Ref. [87].

In this work, we derive black hole solutions in the Hu-Sawicki model of $f(R)$ gravity and study its thermodynamic properties along with its QNMs using the 6th-order WKB method. We compute the shadow radius and present the plots of its variation with respect to different model parameters. The primary motivation for choosing the Hu-Sawicki model is that black hole solutions have not been worked out in this model, and thus it is really intriguing to study the properties of such a solution. The Hu-Sawicki model is a viable choice as it is observationally consistent in cosmological scales [88, 89]. It is consistent with the solar system tests and thus shows viability in the local scales as well [90]. Another reason for choosing this model is that the model parameters of Hu-Sawicki gravity have not been constrained using the available shadow radius data of black holes, although it should be noted that data from cosmological observations have been utilised to constrain this model's parameters. The choice of this model is thus motivated by the gap in the literature and the viability of the model. Some recent articles that utilise the Hu-Sawicki model to study various aspects of astrophysics and cosmology can be found in Refs. [38, 91, 92].

The plan of the paper is as follows. In the second section, we introduce the field equations in the $f(R)$ gravity framework and briefly discuss the method of solving the equations. After attaining the black hole solution, we move to the third section where we compute QNMs of the black hole. Then in the fourth section, we discuss the thermodynamic properties including temperature, entropy and heat capacity along with greybody factors. Then in the fifth section, we compute the shadow radius and plot it for variations in parameters. Finally, we conclude the work with a brief summary and future scopes.

II. FIELD EQUATIONS IN $f(R)$ GRAVITY THEORY

The field equations for the $f(R)$ gravity theory will be presented here in the spherically symmetric spacetime by adopting the metric formalism of the theory, in which the variation of action is done with respect to the metric only. The $f(R)$ gravity field equation can be obtained from an action in which the Ricci scalar R in the Einstein-Hilbert action is replaced by some function $f(R)$ of R . Thus the generic action of the $f(R)$ gravity theory can be written as [60]:

$$S = \frac{1}{2\kappa} \int d^4x \sqrt{-g} f(R) + S_m, \quad (1)$$

where $\kappa = 8\pi Gc^{-4}$ and S_m is the matter part of the action. As mentioned already, taking the variation of the above action (1) with respect to the metric $g_{\mu\nu}$, one can obtain the field equations of $f(R)$ gravity as

$$FR_{\mu\nu} - \frac{1}{2}f(R)g_{\mu\nu} - (\nabla_\mu \nabla_\nu - g_{\mu\nu}\square)F = \kappa T_{\mu\nu}, \quad (2)$$

where $F = df(R)/dR$ and $\square = \nabla_\alpha \nabla^\alpha$. Taking the trace of this (2), we can write the function $f(R)$ as

$$f(R) = \frac{1}{2} (3\square F + FR - \kappa T). \quad (3)$$

The derivative of this Eq. (3) with respect to the radial coordinate r leads to an equation in terms of F and R as given by

$$F'R - FR' + 3(\square F)' = \kappa T', \quad (4)$$

where the prime denotes the derivative with respect to the radial coordinate r . This equation will serve as a consistency relation for the function F that any solution for F must satisfy this relation in order to be a solution of the field equations, Eq. (2). Further, using Eq. (3) in Eq. (2), the field equations can be expressed in terms F instead of $f(R)$ as

$$R_{\mu\nu} - \frac{1}{4}g_{\mu\nu}R = \frac{\kappa}{F} \left(T_{\mu\nu} - \frac{1}{4}g_{\mu\nu}T \right) + \frac{1}{F} \left(\nabla_\mu \nabla_\nu F - \frac{1}{4}g_{\mu\nu}\square F \right). \quad (5)$$

Considering the case of the vacuum where the energy-momentum tensor and its trace vanish, we can rewrite the above equation as

$$FR_{\mu\nu} - \nabla_\mu \nabla_\nu F = \frac{1}{4}g_{\mu\nu}(FR - \square F). \quad (6)$$

Since we are interested in the solution of this time-independent spherically symmetric vacuum field equations following the procedure adopted in Ref. [60], we consider a generic spherically symmetric metric in the form:

$$g_{\mu\nu} = \begin{pmatrix} -N(r) & 0 & 0 & 0 \\ 0 & M(r) & 0 & 0 \\ 0 & 0 & r^2 & 0 \\ 0 & 0 & 0 & r^2 \sin^2 \theta \end{pmatrix}, \quad (7)$$

where $N(r)$ and $M(r)$ are metric coefficients to be determined, associated with the time and space components of the metric respectively which are indeed functions of r . For this spherically symmetric metric, both sides of Eq. (6) become diagonal and accordingly, we can define an index independent parameter from this equation as

$$P_\mu \equiv \frac{FR_{\mu\mu} - \nabla_\mu \nabla_\mu F}{g_{\mu\mu}}. \quad (8)$$

As this quantity P_μ is independent of indices, we can have $P_\mu - P_\nu = 0$ for all μ and ν values and hence from this property one can obtain the following expressions:

$$2F\frac{X'}{X} + rF'\frac{X'}{X} - 2rF'' = 0, \quad (9)$$

$$N'' + \left(\frac{F'}{F} - \frac{X'}{2X} \right) N' - \frac{2}{r} \left(\frac{F'}{F} - \frac{X'}{2X} \right) N - \frac{2}{r^2} N + \frac{2}{r^2} = 0. \quad (10)$$

Here $X = MN$. In this work, our solution is considered to have constant curvature for the sake of simplicity. Hence the terms F' and F'' vanish and the field Eqs. (9) and (10) take the forms:

$$NM' + N'M = 0, \quad (11)$$

$$1 - M + \frac{r}{2} \left(\frac{N'}{N} + \frac{M'}{M} \right) \left(\frac{r}{2} \frac{N'}{N} - 1 \right) - \frac{r^2 N''}{2N} = 0. \quad (12)$$

Solving these two Eqs. (11) and (12), one can obtain:

$$M(r) = \frac{s_1}{N(r)}, \quad \text{and} \quad N(r) = s_1 + \frac{s_2}{r} + s_3 r^2, \quad (13)$$

where s_1 , s_2 and s_3 are constants of integration. In order to get these coefficients, we follow the procedure in Refs. [60, 61] and compare the second solution with the standard Schwarzschild-de Sitter solution. The standard Schwarzschild-de Sitter black hole metric coefficient is [60]

$$C(r) = 1 - \frac{2M}{r} - \frac{\Lambda r^2}{3}. \quad (14)$$

Again, the relationship between the scalar curvature and cosmological constant is [60]

$$R = -4\Lambda. \quad (15)$$

Now, comparing the second solution in Eq. (13) with Eq. (14), we have

$$s_1 = 1, s_2 = -2M, s_3 = -\frac{\Lambda}{3} = \frac{R}{12}.$$

From (3), considering the vacuum case and constant curvature R_0 , we have

$$R_0 = \frac{2f(R_0)}{F(R_0)}. \quad (16)$$

As mentioned earlier, the $f(R)$ gravity model we employed in our work is the Hu-Sawicki model [38], which is given by

$$f(R) = -m^2 \frac{c_1 \left(\frac{R}{m^2}\right)^n}{c_2 \left(\frac{R}{m^2}\right)^n + 1}, \quad (17)$$

where m , $n (> 0)$, c_1 and c_2 are the model parameters. Here c_1 and c_2 are dimensionless and m represents the mass (energy) scale [32]. For this model, we solve Eq. (16) to get the constant curvature

$$R_0 = 12s_3 = m^2 \left(\frac{n-2}{2c_2} \right)^{\frac{1}{n}}. \quad (18)$$

Thus, we arrive at our black hole solution for the Hu-Sawicki model as

$$N(r) = 1 - \frac{2M}{r} + \frac{m^2}{12} \left(\frac{n-2}{2c_2} \right)^{\frac{1}{n}} r^2. \quad (19)$$

It is clear that our black hole solution is independent of the Hu-Sawicki model parameter c_1 . Fig 1 shows the metric function versus radial distance for the other two Hu-Sawicki model parameters m and c_2 , while taking the parameter $n = 1$ for simplicity (this is considered for the whole study if we do not mention otherwise). In the plots, it is seen that the black hole solution (19) has two horizons for a range of parameter values. The first plot shows that with increasing m , the outer horizon moves closer to the inner horizon, while the second plot shows that for higher values of c_2 , the outer horizon increases. After a certain higher value of the parameter m and the lower value of the parameter c_2 , the black hole appears to be a horizonless singularity for the given values of the other parameters.

III. QUASINORMAL MODES OF THE BLACK HOLE

In this section, we compute the QNMs of the black hole (19) using the most common method, the 6th-order WKB approximation method. To this end, we apply a perturbation to the black hole in the form of a probe coupled minimally to a scalar field Φ and having the equation of motion [54]:

$$\frac{1}{\sqrt{-g}} \partial_\alpha \left(\sqrt{-g} g^{\alpha\beta} \partial_\beta \right) \Phi = \mu^2 \Phi, \quad (20)$$

where μ is the mass of the scalar field, which for our convenience will be taken as a massless scalar field with $\mu = 0$. We can express the scalar field Φ in terms of spherical harmonics of the form [54]:

$$\Phi(t, r, \theta, \phi) = e^{-i\omega t} \frac{\Psi(r)}{r} Y_l^p(\theta, \phi). \quad (21)$$

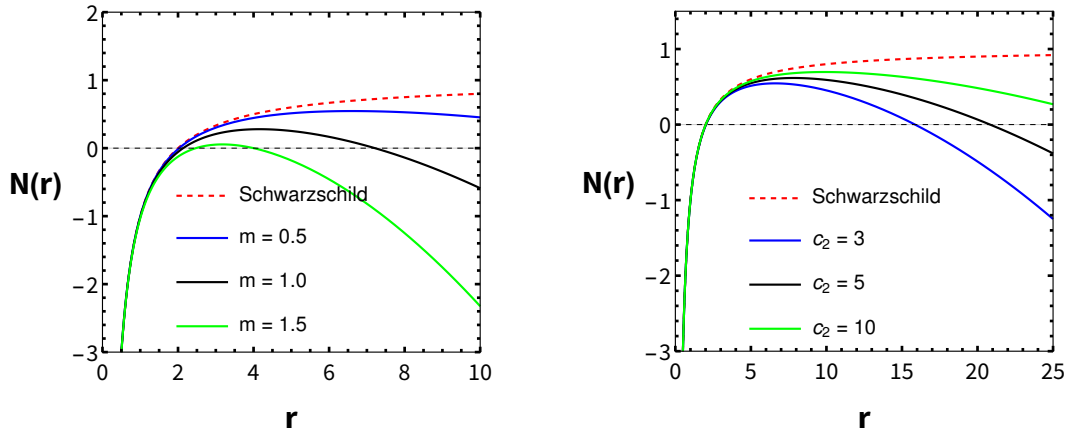


FIG. 1. Black hole metric function versus radial distance r for different values of parameters. In the left plot, we use $c_2 = 3$ and $n = 1$ while in the right plot, we use $m = 0.5$ and $n = 1$. The red dashed line shows the ideal Schwarzschild case.

Here $\Psi(r)$ represents the radial part of the wave and Y_l^p represents the spherical harmonic part. Employing Eq. (21) in Eq. (20), we get a Schrödinger-type equation, as given below:

$$\frac{d^2\Psi}{dx^2} + [\omega^2 - V(x)] \Psi = 0, \quad (22)$$

with the new variable, the tortoise coordinate, which is defined as

$$x = \int \frac{dr}{N(r)}. \quad (23)$$

The effective potential in Eq. (22) can be expressed as

$$V(r) = N(r) \left(\frac{N'(r)}{r} + \frac{l(l+1)}{r^2} \right). \quad (24)$$

It is necessary to apply the appropriate boundary conditions to Eq. (22) for the physical consistency both at the black hole horizon and at infinity. For spacetime which is flat asymptotically the following quasinormal criteria have to be satisfied:

$$\Psi(x) \rightarrow \begin{cases} Ae^{+i\omega x} & \text{if } x \rightarrow -\infty, \\ Be^{-i\omega x} & \text{if } x \rightarrow +\infty \end{cases}. \quad (25)$$

Here, the coefficients A and B represent the amplitudes of the waves. These ingoing and outgoing waves are in accordance with the physical requirements that nothing can escape from the black hole horizon and no radiation comes from the infinity respectively. Further, these make sure of the existence of an infinite set of discrete complex numbers, usually known as the QNMs.

To study the behaviour of the potential (24) before calculating the QNMs of the black hole (19), we plot the potential versus r for different variations of model parameters in Fig. 2. As seen from the left plot of Fig. 2, the peak of the potential decreases for higher m values. From the middle plot, one can see that increasing values of parameter c_2 enhances the peak of the potential. A similar trend is seen with multipole l values, where peaks are found to increase for higher l values.

The QNMs have been calculated utilising the 6th-order WKB method in the form of their amplitude and damping varying with the model parameters. As seen from Fig. 3, the general trend of amplitude and damping of QNMs is that both decrease with the parameter m for all values of multiple l . On the other hand, Fig. 4 shows that both amplitude and damping increase slightly with the parameter c_2 for all l values. In both cases, the effect of l is more dominating on the amplitude than that on the damping. Moreover, in both cases of m and c_2 variations, the amplitude increases, while the damping decreases with the increasing value of l .

We compute the error associated with the WKB QNMs with a prescribed formula that has been used extensively in the literature. This error estimating formula for the WKB method is as follows [54, 76, 77]:

$$\Delta_6 = \frac{|WKB_7 - WKB_5|}{2}, \quad (26)$$

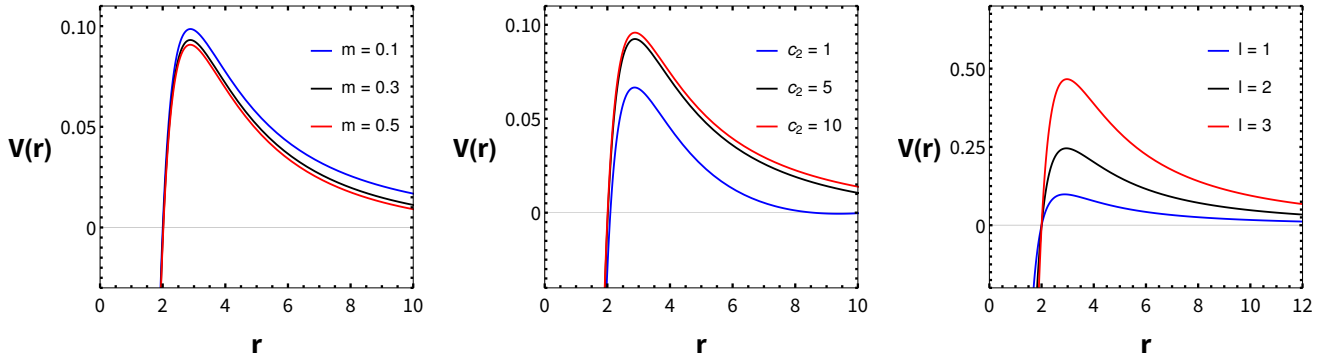


FIG. 2. Behaviours of black hole potential with respect to radial distance r for different model parameters. The left plot uses values of $c_2 = 2$, $n = 1$ and multipole $l = 1$. The middle plot uses $m = 0.5$, $n = 1$ and multipole $l = 1$. The right plot uses $m = 0.1$, $n = 1$ and $c_2 = 2$.

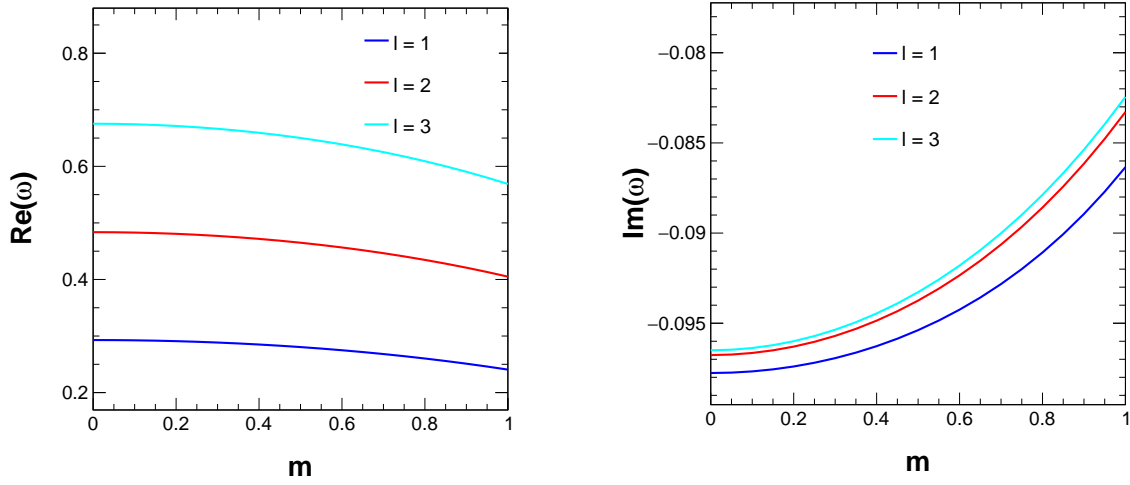


FIG. 3. Variation of amplitude and damping of QNMs with respect to parameter m for three values of multipole l . Here we use $n = 1$, $M = 1$ and $c_2 = 4$ to represent the features of QNMs.

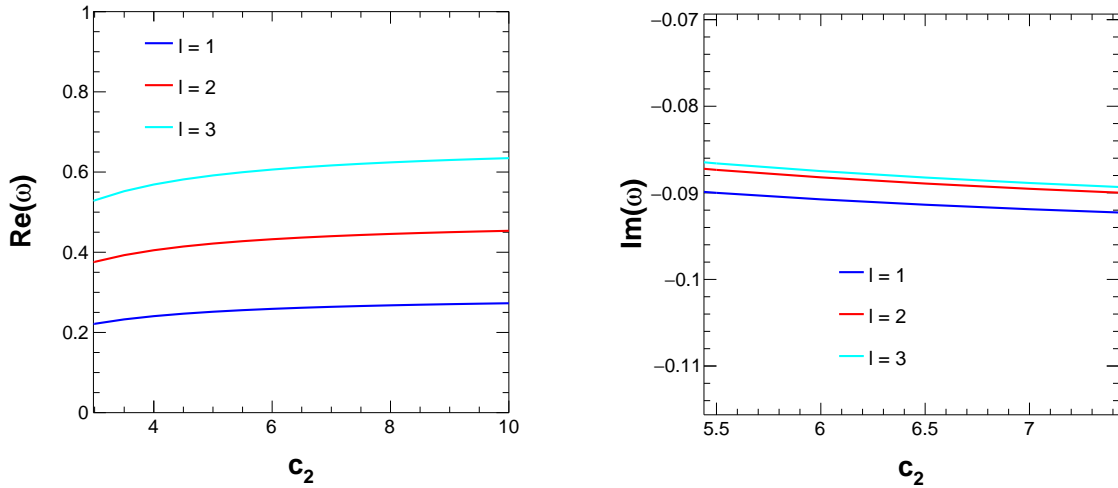


FIG. 4. Variation of amplitude and damping of QNMs with respect to parameter c_2 for three values of multipole l . Here parameters $n = 1$, $M = 1$ and $m = 1$ have been used.

where WKB_5 and WKB_7 are respectively the QNMs obtained from the 5th and 7th order WKB method. In Table I, we present

the 6th-order WKB QNMs along with the associated errors for various values of the model parameters along with the multipole number l . It is clear that the errors are reduced for higher multipole numbers l . Similar trends in variations of QNMs with respect to different parameters as seen in Figs. 3 and 4 are displayed in the tabulated data. The estimated errors in most of the cases lie around $10^{-4} - 10^{-5}$.

TABLE I. 6th-order WKB QNMs of the black hole specified by the metric function (19) for the multipoles $l = 1, 2, 3$ with $n = 0$ and for different values of the model parameters. The estimated errors associated with the WKB results have also been shown. The QNMs with $m = c_2 = 0$ represent the Schwarzschild case, which are listed for the comparison purpose only.

Multipole	m	c_2	6th order QNMs	Δ_6
$l = 1$	0.0	0.0	0.292910 - 0.097762i	0.9824×10^{-6}
	0.1	4.0	0.292420 - 0.097672i	0.9871×10^{-4}
	0.3	4.0	0.288479 - 0.096937i	0.9483×10^{-4}
	0.5	4.0	0.280478 - 0.0953844i	0.9076×10^{-4}
	1.0	4.0	0.240646 - 0.0863446i	0.6341×10^{-4}
	1.0	6.5	0.261572 - 0.0913734i	0.7809×10^{-4}
$l = 2$	0.0	0.0	0.483642 - 0.096766i	0.8364×10^{-7}
	0.1	4.0	0.482906 - 0.0966493i	0.8355×10^{-5}
	0.3	4.0	0.476986 - 0.0957027i	0.7845×10^{-5}
	0.5	4.0	0.46497 - 0.0937446i	0.7326×10^{-5}
	1.0	4.0	0.405024 - 0.0832849i	0.5689×10^{-5}
	1.0	6.5	0.436572 - 0.0889274i	0.6718×10^{-5}
$l = 3$	0.0	0.0	0.675366 - 0.096501i	0.1032×10^{-7}
	0.1	4.0	0.674374 - 0.096375i	0.1534×10^{-5}
	0.3	4.0	0.666393 - 0.095361i	0.1534×10^{-5}
	0.5	4.0	0.65018 - 0.0932773i	0.1527×10^{-5}
	1.0	4.0	0.568930 - 0.082446i	0.5235×10^{-6}
	1.0	6.5	0.611771 - 0.088233i	0.1033×10^{-5}

IV. THERMODYNAMIC CHARACTERISTICS OF THE BLACK HOLE

As mentioned earlier, a black hole as a thermodynamic system was first conceptualised in the ground-breaking work of Hawking and Bekenstein in the early 1970s. In this paper, we analyse the black hole temperature and the grey body factors which are important properties that give useful insights in this regard. The temperature of a black hole is an important property that is associated with the quantum particles created near its horizon. It is inversely related to the size or mass of the black hole, that is a larger black hole will have a lower temperature. Hawking conceptualised the temperature of black hole in the form of radiation, which is today referred to as Hawking radiation. It remains a challenge to detect such radiation experimentally. We can theoretically compute the black hole temperature from the metric solution (19), by employing the simple relation:

$$T_{BH} = \frac{N'(r)}{4\pi} = \frac{1}{4\pi r_H^2} \left[2M + \frac{m^2}{12} \left(\frac{n-2}{c_2} \right)^{\frac{1}{n}} r_H^3 \right]. \quad (27)$$

It can also be calculated using the First law of black hole thermodynamics as follows:

$$T_{BH} = \frac{dM}{dS} = \frac{dM'}{dS'} = \frac{1}{4\pi r_H^2} \left[2M + \frac{m^2}{12} \left(\frac{n-2}{c_2} \right)^{\frac{1}{n}} r_H^3 \right]. \quad (28)$$

This confirms our computation of the black hole temperature from the first law. We plot the thermodynamic temperature (27) with respect to the horizon radius r_H in Fig. 5. Here, we see clearly that with horizon radius r_H , the temperature of the black hole is always in the decreasing trend. The left plot shows the temperature variations with respect to r_H for three different values of parameter m . It is seen that higher values of m lead to negative temperatures. While for the parameter c_2 , lower values lead

to negative temperatures as can be seen from the right panel of Fig. 5. Though the negative temperature seems unphysical, this has been encountered in the literature and explained as a possible state of formation of ultra-cold black holes [54, 80]. Negative temperatures may also suggest that the black hole is thermodynamically unstable [93].

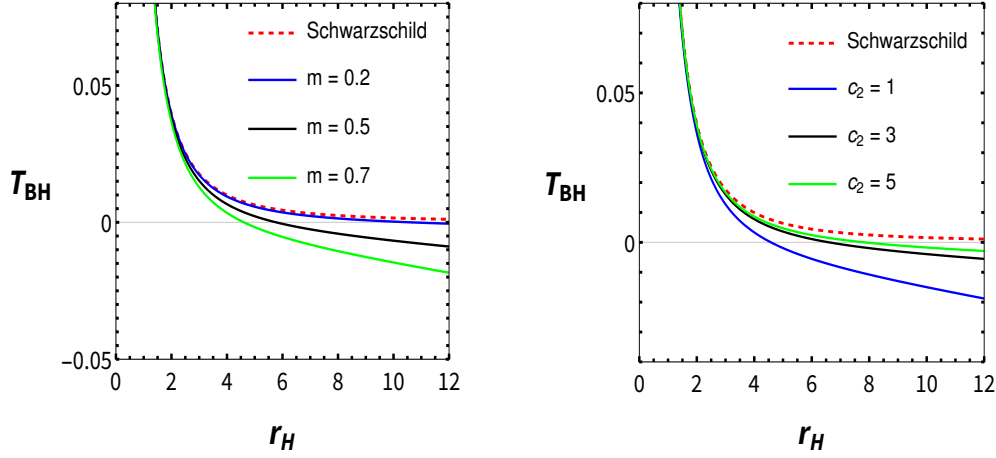


FIG. 5. Variation of temperature versus r_H for three different values of m on the left plot and for three different values of c_2 on the right plot. For the left plot, we use $n = M = 1$ and $c_2 = 2$, while for the right plot, we use $M = n = 1$ and $m = 0.5$.

To study the thermodynamic stability of the black hole solution, we have computed the heat capacity of the solution. Following the first law of black hole thermodynamics, the formula for calculating the heat capacity of the black hole can be found as:

$$C_{BH} = \frac{dM}{dT} = 3\pi r^2 \left(\frac{4(6M + r)}{m^2 r^3 \left(\frac{n-1}{c_2}\right)^{1/n} - 24M} + 1 \right). \quad (29)$$

The plots of the heat capacity of the black hole for different values of the model's parameters are shown in Fig. 6. Here we have considered the constraint values of the model's parameters that are obtained from the shadow analysis as can be seen from Fig. 9. In the left hand plot of Fig. 6, we have used $m = 0.5$ and $c_2 = 2$, which are the extreme bounds obtained from shadow radius. It is seen that when $r_H \geq 8$, the heat capacity takes positive values, otherwise it remains negative. In the right hand plot of the same figure, we have used intermediate values of the parameters in the viable range suggested by shadow analysis. It is seen from this plot that the heat capacity always remains negative, which indicates thermodynamic instability. Thus we may comment that the black hole is mostly thermodynamically unstable.

The greybody factor or the transmission coefficient is a measure of the probability that a particle created by quantum processes near the event horizon of a black hole will escape to infinity or get absorbed inside the black hole. Greybody factor (T^2) equal to 1 means that all the particles that are created are able to escape the black hole while lower values of it mean that some of them end up inside it. If $T^2 = 0$, it means that the black hole is completely dark and absorbs every single particle. The greybody

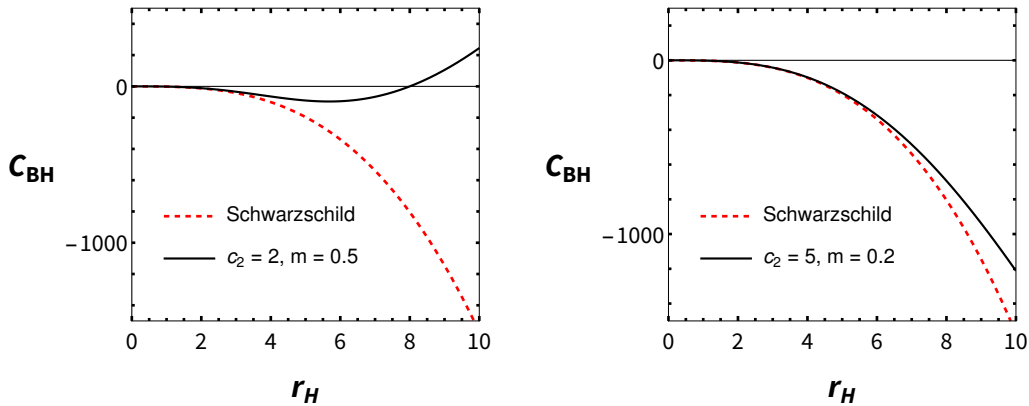


FIG. 6. Heat capacity of the black hole versus horizon radius is shown. The left plot shows that for $r_H \geq 8$, the heat capacity takes positive values, otherwise the heat capacity remains negative. It indicates the black hole is thermodynamically unstable in most of the parameter space.

factor has been extensively studied in the literature in various scenarios. We can express the reflection and transmission of the particles hitting the black hole barrier potential in the following form [94]:

$$\psi(x) = T(\omega) \exp(-i\omega x), \quad x \rightarrow -\infty, \quad (30)$$

$$\psi(x) = \exp(-i\omega x) + R(\omega) \exp(i\omega x), \quad x \rightarrow +\infty, \quad (31)$$

where $R(\omega)$ and $T(\omega)$ are respectively reflection and transmission coefficients and are functions of frequency ω . WKB approximation formula is used to get to the computational form of these two coefficients which are presented below [94]:

$$|R(\omega)|^2 = \frac{1}{1 + \exp(-2\pi i\tau)}, \quad (32)$$

$$|T(\omega)|^2 = \frac{1}{1 + \exp(2\pi i\tau)}, \quad (33)$$

where the parameter τ is defined in the WKB method as the following [94]:

$$\tau = \frac{i(\omega^2 - V_0)}{\sqrt{-2V_0''}} - \Lambda_j. \quad (34)$$

Here double primes represent the double derivative of the maximum of the effective potential V_0 with respect to x and Λ_j can be obtained from the WKB formula found in Ref. [79]. In Fig. 7, we plot the greybody factors with respect to frequency ω for three values of the model parameters m considering $n = 1$, $c_2 = 1$ and $M = 1$ with multipole $l = 1$ (left plot) and $l = 2$ (right plot). It is seen that for higher m values the greybody factor increases faster with respect to ω than that for smaller m values. Also, for a smaller l value ($l = 1$), the greybody factor increase is more rapid and begins from a smaller ω value as compared to a higher l value ($l = 2$). It needs to be mentioned that the values of the parameter c_2 are found to be insensitive in the variation of the greybody factors with respect to ω as shown in Fig. 7.

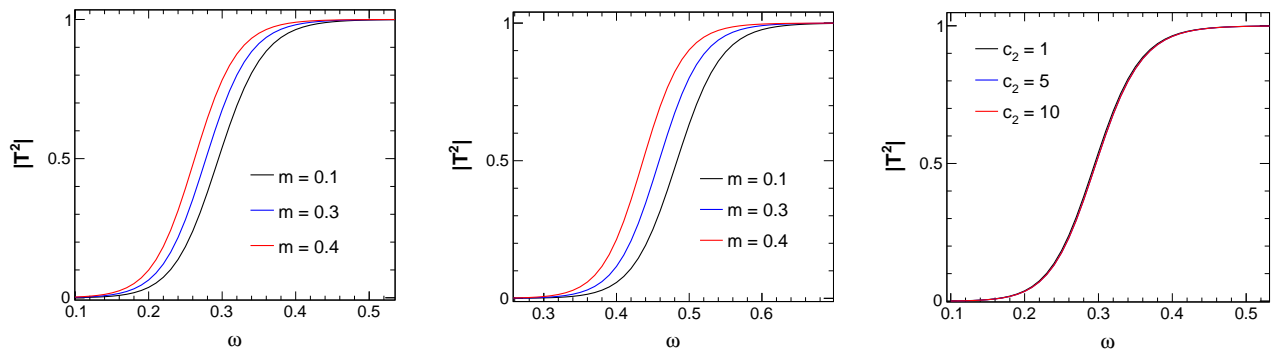


FIG. 7. Greybody factors versus frequency ω for different values of m with $l = 1$ (left plot) and $l = 2$ (right plot). We have used $M = n = 1$ and $c_2 = 1$ in the first two plots and $m = 0.1$ for the third plot. The third plot shows that greybody factor is independent of parameter c_2 .

V. SHADOW OF THE BLACK HOLE

Black hole shadow has been extensively studied in the literature as it provides good scope to test various theories of gravity and black hole physics in extreme gravity regimes. The recent observational data of black hole shadow radius has provided the scientific community an opportunity to constrain model parameters using these data. In this section, we compute the photon sphere and the shadow radius expression and plot the same for analysing its dependence on various model parameters. We also try to constrain the parameter space with observational data of the EHT group.

The simple condition to determine the photon sphere radius of a black hole in spherical symmetry consideration is given by the following relation [71, 72]:

$$2 - \frac{rN'(r)}{N(r)} = 0. \quad (35)$$

Using the form of $N(r)$ from Eq. (19), we solve the Eq. (35) for r to get the photon sphere radius as

$$r_{ph} = 3M. \quad (36)$$

From the photon radius, we can derive the shadow radius as follows:

$$r_{sh} = \frac{r_{ph}}{\sqrt{N(r)|_{r \rightarrow r_{ph}}}} = \frac{3M}{\sqrt{\frac{3}{4}m^2M^2 \left(\frac{n-2}{2c_2}\right)^{1/n} + \frac{1}{3}}}. \quad (37)$$

Obviously, the shadow radius depends on all three model parameters associated with $N(r)$. It is also evident that when model parameters $m = n = c_2 = 0$, we recover the standard $r_{sh} = 3\sqrt{3}M$ which is the shadow radius for the Schwarzschild black hole. Now, for the 2-D stereoscopic projection of shadow radius, we define celestial coordinates X and Y as given by [71, 72]

$$X = \lim_{r_0 \rightarrow \infty} \left(-r_0^2 \sin \theta_0 \frac{d\phi}{dr} \Big|_{r_0} \right), \quad (38)$$

$$Y = \lim_{r_0 \rightarrow \infty} \left(r_0^2 \frac{d\theta}{dr} \Big|_{(r_0, \theta_0)} \right). \quad (39)$$

Here θ_0 is the observer's angular position with regards to the plane of the black hole. In Fig.8, we show the variation of the shadow radius with parameters m and c_2 . It is seen from the left plot that with an increase in m , the shadow radius increases. In the right plot, it is evident that the shadow radius decreases with increasing c_2 values. Thus, the parameters m and c_2 have opposite influences on the shadow radius.

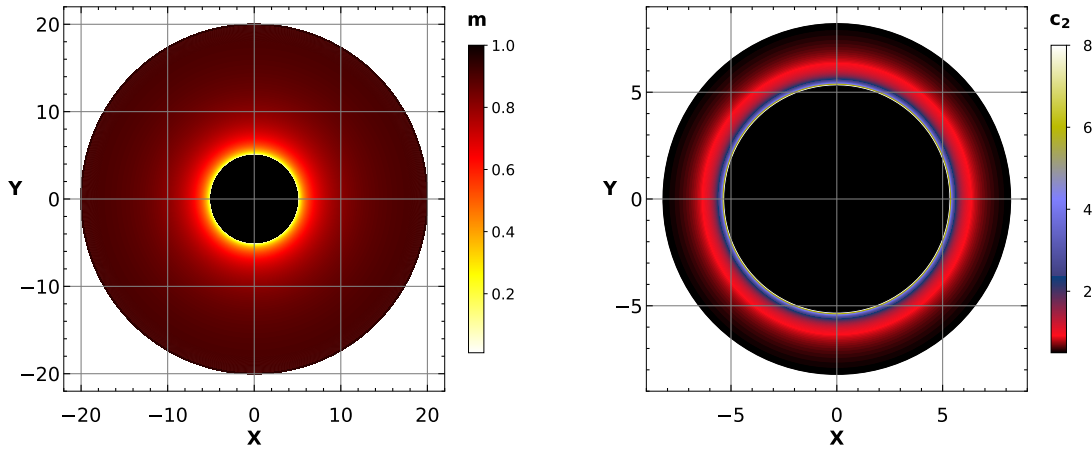


FIG. 8. Stereoscopic projection of shadow radius in terms of celestial coordinates. The left plot is for the variation of m with parameters $c_2 = M = n = 1$ and the right plot is for the variation of c_2 with $M = n = 1$ and $m = 0.1$

In order to constrain the parameters of the model, we shall employ the technique mentioned in Ref. [71]. We briefly present some important steps in this direction. The main point of the methodology is that we compare the observed angular radius of the Sgr A* black hole as captured by the EHT group recently with the theoretically calculated shadow radius from the expression (37) by constraining the model parameters. This requires the prior value of the mas-to-distance ratio for Sgr A*. Another feature that is required for this method is the calibration factor that correlates the observed to the calculated shadow radius. This method has been used to constrain model parameters in the literature [95–97] and we shall follow the same route.

A new parameter δ defined by the EHT group to refer to the fractional deviation between the observed shadow radius r_s and shadow radius of a Schwarzschild black hole r_{sch} is [71]

$$\delta = \frac{r_s}{r_{sch}} - 1 = \frac{r_s}{3\sqrt{3}M} - 1. \quad (40)$$

This parameter was estimated by the Keck and VLTI measurements as [71]

$$\text{Keck} : \delta = -0.04^{+0.09}_{-0.10}$$

$$\text{VLTI} : \delta = -0.08^{+0.09}_{-0.09}$$

For simplification, we shall adopt the mean of the two observations as considered in Ref. [71] in the rest of the work, which is

$$\delta = -0.060 \pm 0.065. \quad (41)$$

This leads to δ parameter's 1σ and 2σ intervals as

$$-0.125 \lesssim \delta \lesssim 0.005 \quad (1\sigma), \quad (42)$$

$$-0.190 \lesssim \delta \lesssim 0.070 \quad (2\sigma). \quad (43)$$

It is found that the bounds (42) and (43) when imposed upon Eq. (40) give the bounds on r_{sh} as follows [71]:

$$4.55 \lesssim r_{sh}/M \lesssim 5.22 \quad (1\sigma), \quad (44)$$

$$4.21 \lesssim r_{sh}/M \lesssim 5.56 \quad (2\sigma). \quad (45)$$

We plot the shadow radius with the bounds imposed by the observations of Keck and VLTI in Fig. 9. The left plot shows that the shadow radius increases with increasing m values as found in Fig. 8. It shows that for smaller values of c_2 , the shadow radius quickly moves to the forbidden region. With increasing c_2 values, the shadow radius within the allowed region increases. In the right plot, the shadow radius is plotted versus c_2 which shows that the shadow radius decreases with increasing c_2 values as observed earlier. The plots are within the 2σ allowed region in this case with the exception of larger m and smaller c_2 values as clearly visible from the plot. It is quite evident that the constraints imposed are not rigid but depend on the range of values of the parameters of the model.

This method of constraining parameters of a theory has been adopted in the literature [95, 96] and by the EHT group themselves [97] and provides a robust way of constraining parameters. But in cases of model parameters exceeding one, we need some supporting constraining methods so that one parameter can be cornered and rigorous constraints can be obtained. However, we leave this as a future extension of the work.

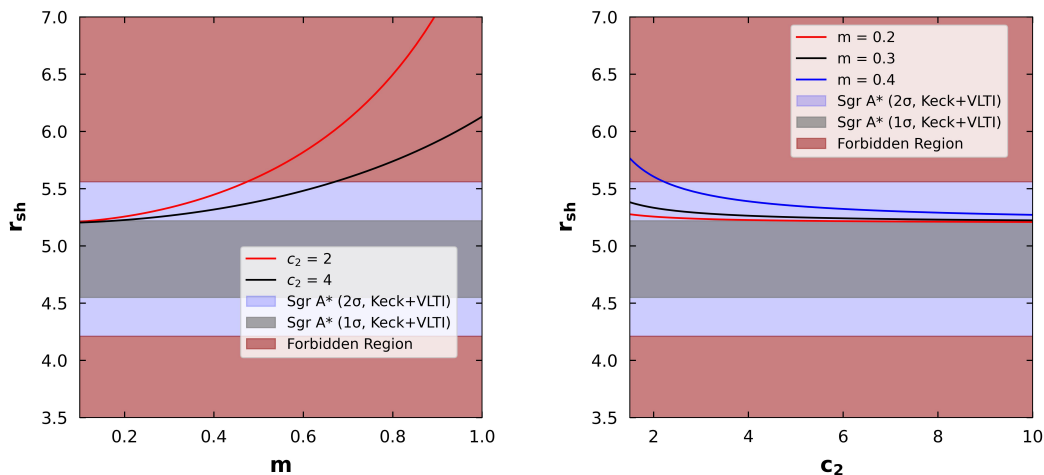


FIG. 9. Shadow radius versus parameter m and c_2 have been plotted in the background of Keck and VLTI constrains [71] from observations of Sgr A*. We have chosen $M = 1$ and $n = 1$ for these plots. The red portion represents the zone forbidden by Keck-VLTI observation.

VI. CONCLUSION

In this work, we derive novel black hole solutions in the framework of Hu-Sawicki gravity. We plot the metric function versus r for various values of model parameters and encountered two horizons of the black hole. It is seen that higher m values cause the horizon radius to shrink while opposite trend is observed for parameter c_2 . We then analyse the QNMs of the novel black hole solution with 6th order WKB approximation. The amplitude increases with increase in c_2 while it decreases with m . The damping decreases with increasing m while it increases slightly with c_2 . This trend can be realised from the tabulated QNM data in Table I. It is evident that the QNM frequencies are affected by the model parameters. The associated error is found to be around 10^{-4} to 10^{-5} in some cases.

Thermodynamic temperature associated with the black hole is investigated and it is found to decrease with r_H in all cases. The temperature can also become negative, suggesting the possibility of formation of ultra-cold black hole. The heat capacity of

the black hole has been computed and plotted the same with respect to the horizon radius. It is seen that the heat capacity takes negative values for most of the parameter space, indicating thermodynamic instability of the obtained black hole solution. The greybody factors are also computed, specially the transmission coefficients with respect to frequency ω and the dependence of the model parameter m is studied. Higher m results in swifter increase in the greybody factors towards saturation value of 1. It is noteworthy that increasing the multipole l lowers the rate of increase of greybody factors and saturation is achieved at higher ω .

The photon radius and the shadow radius associated with the spherically symmetric black hole spacetime are then studied. We presented the stereographic projection of the shadow in celestial coordinate system and using contour-type feature, showed the variation of the shadow radius with increasing model parameters m and c_2 . Using the already established constraints on r_{sh} by Keck and VLTI observations, we constrain our model parameters using a well proven scheme. The parameter m is roughly constrained to be less than ~ 0.5 while parameter c_2 is constrained to be greater than ~ 2 , as can be seen from Figure 9.

The recent technical advancements made in the fields of astrophysics and observational astronomy has made the present era very suitable for theoretical physicists to constrain and test fundamental theories and models, which was not possible until a decade back. With ground-breaking leaps in the form of LIGO-Virgo team's observation of Gravitational Waves in 2015 along with the first-ever image of the black hole M87* and later that of Sgr A*, scientists plan to further enhance sensitivity of the present detectors as well as new ambitious projects like the space-based LISA project and the Einstein Telescope are already in the planning stages. As a future scope of this work, we can analyse other viable models of gravity like $f(R, T)$ and $f(Q)$ and work on new black hole solutions as well as rotating Kerr-type solutions can also be explored. The study of black hole shadows surely holds a lot of potential in constraining fundamental physics and it certainly deserves further investigation.

ACKNOWLEDGEMENTS

UDG is thankful to the Inter-University Centre for Astronomy and Astrophysics (IUCAA), Pune, India for awarding the Visiting Associateship of the institute.

-
- [1] R.M. Wald, *General Relativity*, The University of Chicago Press, Chicago, 1984.
 - [2] C. M. Will, *Was Einstein right? A centenary assessment*, arXiv:1409.7871 [gr-qc] (2004).
 - [3] C. M. Will, *New General Relativistic Contribution to Mercury's Perihelion Advance*, *Phys. Rev. Lett.* **120**, 191101 (2018).
 - [4] C. M. Will, *The 1919 measurement of the deflection of light*, *Class. Quantum Grav.* **32**, 124001 (2015).
 - [5] B. P. Abbott et al., *Observation of Gravitational Waves from a Binary Black Hole Merger*, *Phys. Rev. Lett.* **116**, 061102 (2016).
 - [6] B. P. Abbott et al., *Observation of Gravitational Waves from a 22-Solar-Mass Binary Black Hole Coalescence*, *Phys. Rev. Lett.* **116**, 241103 (2016).
 - [7] B. P. Abbott et al., *Observation of Gravitational Waves from a Binary Neutron Star Inspiral*, *Phys. Rev. Lett.* **119**, 161101 (2017).
 - [8] B. P. Abbott et al., *Observation of a Binary-Black-Hole Coalescence with Asymmetric Masses*, *Phys. Rev. D* **102**, 043015 (2020).
 - [9] R. Abbott et al., *Observation of Gravitational Waves from Two Neutron Star-Black Hole Coalescences*, *ApJL* **915**, L5 (2021).
 - [10] The Event Horizon Telescope Collaboration et al., *First M87 Event Horizon telescope Results. I. The Shadow of the supermassive Black Hole*, *ApJL* **875**, L1 (2019).
 - [11] The Event Horizon Telescope Collaboration et al., *First M87 Event Horizon telescope Results. II. Array and Instrumentation*, *ApJL* **875**, L2 (2019).
 - [12] The Event Horizon Telescope Collaboration et al., *First M87 Event Horizon telescope Results. III. Data Processing and Calibration*, *ApJL* **875**, L3 (2019).
 - [13] The Event Horizon Telescope Collaboration et al., *First M87 Event Horizon telescope Results. IV. Image the Central Supermassive Black Hole*, *ApJL* **875**, L4 (2019).
 - [14] The Event Horizon Telescope Collaboration et al., *First M87 Event Horizon telescope Results. V. Physical Origin of the Asymmetric Ring*, *ApJL* **875**, L5 (2019).
 - [15] The Event Horizon Telescope Collaboration et al., *First M87 Event Horizon telescope Results. VI. The Shadow and Mass of the Central Black Hole*, *ApJL* **875**, L6 (2019).
 - [16] V. Faraoni and S. Capozziello, *Beyond Einstein gravity: a survey of gravitational theories for cosmology and astrophysics*, *Fundam. Theor. Phys.* **170**, 1-428 (2010).
 - [17] A. G. Riess et al., *Observational Evidence from Supernovae for an Accelerating Universe and a Cosmological Constant*, *The Astronomical Journal* **116**, 1009 (1998).
 - [18] S. Perlmutter et al., *Measurements of Ω and Λ from 42 High-Redshift Supernovae*, *ApJ* **517**, 565 (1999)
 - [19] C. Pérez de los Heros, Status, Challenges and Directions in Indirect Dark Matter Searches, *Symmetry* **12**, 1648 (2020).
 - [20] N. A. Bahcall, *The Cosmic Triangle: Revealing the State of the Universe*, *Science* **284**, 1481 (1999).
 - [21] L. Amendola and S. Tsujikawa, *Dark Energy: Theory and Observations*, Cambridge University Press, Cambridge, 2010.
 - [22] D. J. Gogoi and U. D. Goswami, *A new $f(R)$ gravity model and properties of gravitational waves in it*, *EPJC* **80**, 1101 (2020).
 - [23] T. P. Sotiriou and V. Faraoni, *$f(R)$ theories of gravity*, *Rev. Mod. Phys.* **82**, 451 (2010).

- [24] T. P. Sotiriou and V. Faraoni, *f(R) theories of gravity*, *Rev. Mod. Phys.* **82**, 451 (2010).
- [25] A. De Felice and S. Tsujikawa, *f(R) Theories*, *Living Rev. Relativ.* **13**, 3 (2010).
- [26] T. Harko, F. S. N. Lobo, S. Nojiri and S. D. Odintsov, *f(R,T) gravity*, *Phys. Rev. D* **84**, 024020 (2011).
- [27] P. Sarmah, A. De and U. D. Goswami, *Anisotropic LRS-BI Universe with f(Q) gravity theory*, *Phys. Dark Universe* **40**, 101209 (2023).
- [28] A. De, S. Mandal, J. T. Beh, T. H. Loo and P. K. Sahoo, *Isotropization of locally symmetric Bianchi-I universe in f(Q)-gravity*, *EPJC* **82**, 10052 (2022).
- [29] R. Solanki, A. De, S. Mandal and P. K. Sahoo, *Accelerating expansion of the universe in modified symmetric teleparallel gravity*, *Phys. Dark Universe* **36**, 101053 (2022).
- [30] D. J. Gogoi, A. Övgün and M. Koussour, *Quasinormal Modes of Black holes in f(Q) gravity*, *EPJC* **83**, 700 (2023).
- [31] T. P. Sotiriou and V. Faraoni, *f(R) theories of gravity*, *Rev. Mod. Phys.* **82**, 451 (2010).
- [32] N. Parbin and U. D. Goswami, *Scalars mimicking dark matter in the Hu-Sawicki model of f(R) gravity*, *Mod. Phys. Lett. A* **36**, 37 (2021).
- [33] N. Parbin and U. D. Goswami, *Galactic rotation dynamics in a new f(R) gravity model*, *EPJC* **83**, 411 (2023).
- [34] R. Myrzakulov, *Accelerating universe from F(T) gravity*, *EPJC* **71**, 1752 (2011).
- [35] A. Mukherjee and N. Banerjee, *Acceleration of the universe in f(R) gravity models*, *Astrophys. Space Sci.* **352**, 839 (2014).
- [36] P. Rastall, *Generalization of the Einstein Theory*, *Phys. Rev. D* **6**, 3357 (1972).
- [37] A. A. Starobinsky, *Disappearing cosmological constant in f(R) gravity*, *JETP* **86**, 157 (2007).
- [38] W. Hu and I. Sawicki, *Models of f(R) cosmic acceleration that evade solar system tests*, *Phys. Rev. D* **76**, 064004 (2007).
- [39] R. Saffari and S. Rahvar, *f(R) Gravity: From the Pioneer Anomaly to the Cosmic Acceleration*, *Phys. Rev. D* **77**, 104028 (2008).
- [40] J. -Y. Cen, S. -Y. Chien, C. -Q. Geng and C. -C. Lee, *Cosmological evolutions in Tsujikawa model of f(R) Gravity*, *Phys. Dark Universe* **26**, 100375 (2019).
- [41] D. J. Gogoi and U. D. Goswami, *A new f(R) gravity model and properties of gravitational waves in it*, *EPJC* **80**, 1011 (2020).
- [42] P. Bessa, M. Campista and A. Bernui, *Observational constraints on Starobinsky f(R) cosmology from cosmic expansion and structure growth data*, *EPJC* **82**, 506 (2022).
- [43] P. V. Ky, N. T. H. Van and N. A. Ky, *Gravitational radiation of a spherically symmetric source in f(R)-gravitation*, *EPJC* **84**, 298 (2024).
- [44] J. Bora, D. J. Gogoi and U. D. Goswami, *Strange stars in f(R) gravity palatini formalism and gravitational wave echoes from them*, *JCAP* **09**, 057 (2022).
- [45] L. Amendola, R. Gannouji, D. Polarski and S. Tsujikawa, *Conditions for the cosmological viability of f(R) dark energy models*, *Phys. Rev. D* **75**, 083504 (2007).
- [46] P. Sarmah and U. D. Goswami, *Dynamical system analysis of LRS-BI Universe with f(Q) gravity theory*, [arXiv:2403.16118v1 \[gr-qc\]](https://arxiv.org/abs/2403.16118v1)
- [47] T. Katuragawa, S. Matsuzaki and E. Senaha, *F(R) gravity in the early Universe: electroweak phase transition and chameleon mechanism**, *Chinese Physics C* **43**, 105101 (2019).
- [48] R. Solanki, A. De, S. Mandal and P. K. Sahoo, *Accelerating expansion of the universe in modified symmetric teleparallel gravity*, *Phys. Dark Universe* **36**, 101053 (2022).
- [49] S. Capozziello, V. De Falco and C. Ferrara, *Comparing equivalent gravities: common features and differences*, *EPJC* **82**, 856 (2023).
- [50] D. Zhao, *Covariant formulation of f(Q) theory*, *EPJC* **82**, 303 (2022).
- [51] K. Schwarzschild, *On the gravitational field of a mass point according to Einstein's theory*, [arXiv:physics/9905030](https://arxiv.org/abs/physics/9905030) (1916).
- [52] S. Fernando, *Schwarzschild black hole surrounded by quintessence: null geodesics*, *Gen. Relativ. Gravit.* **44**, 1857–1879 (2012).
- [53] R. Karmakar, D. J. Gogoi and U. D. Goswami, *Quasinormal modes and thermodynamic properties of GUP-corrected Schwarzschild black hole surrounded by quintessence*, *IJMPA* **37**, 2250180 (2022).
- [54] D. J. Gogoi, R. Karmakar and U. D. Goswami, *Quasinormal Modes of Non-Linearly Charged Black Holes surrounded by a Cloud of Strings in Rastall Gravity*, *IJGMMP* **20**, 2350007 (2023).
- [55] S. Chen, B. Wang and R. Su, *Hawking radiation in a d-dimensional static spherically symmetric black hole surrounded by quintessence*, *Phys. Rev. D* **77**, 124011 (2008).
- [56] Y. Heydarzade and F. Darabi, *Black Hole Solutions Surrounded by Perfect Fluid in Rastall Theory*, *Phys. Lett. B* **771**, 365 (2017).
- [57] F. Atamurotov, A. Abdurajbarov and W. -B. Han, *Effect of plasma on gravitational lensing by a Schwarzschild black hole immersed in perfect fluid dark matter*, *Phys. Rev. D* **104**, 084015 (2021).
- [58] R. A. Konoplya, *Shadow of a black hole surrounded by dark matter*, *Phys. Lett. B* **795**, 1 (2019).
- [59] R. Karmakar, D. J. Gogoi and U. D. Goswami, *Thermodynamics and Shadows of GUP-corrected Black Holes with Topological Defects in Bumblebee Gravity*, *Phys. Dark Universe* **41**, 101249 (2023).
- [60] T. Multamäki and I. Vilja, *Spherically symmetric solutions of modified field equations in f(R) theories of gravity*, *Phys. Rev. D* **74**, 064002 (2006).
- [61] B. Hazarika and P. Phukon, *Thermodynamic Topology of Black Holes in f(R) Gravity*, *PTEP* **2024**, Issue 4, 043E01 (2024).
- [62] V. Prokopov, S. Alexeyev and O. Zenin, *Black Hole Shadows Constrain Extended Gravity*, *J. Exp. Theor. Phys.* **135**, 91–99 (2022).
- [63] K. Jafarzade, M. K. Zangeneh and F. S. N. Lobo, *Observational optical constraints of regular black holes*, *Annals of Physics* **446**, 169126 (2022).
- [64] İ. Çimdiker, D. Demir, and A. Övgün, *Black Hole Shadow in Symmergent Gravity*, *Physics of the Dark Universe* **34**, 100900 (2021).
- [65] S. Haroon, K. Jusufi and M. Jamil, *Shadow Images of a Rotating Dyonic Black Hole with a Global Monopole Surrounded by Perfect Fluid*, *Universe* **6** (2), 23 (2020).
- [66] M. Okyay and A. Övgün, *Nonlinear electrodynamics effects on the black hole shadow, deflection angle, quasinormal modes and greybody factors*, *JCAP* **01**, 009 (2022).
- [67] A. Belhaj and Y. Sekhmani, *Shadows of rotating quintessential black holes in Einstein–Gauss–Bonnet gravity with a cloud of strings*, *Gen. Relativ. Gravit.* **54** (2021).
- [68] R. Roy, S. Vagnozzi and L. Visinelli, *Superradiance evolution of black hole shadows revisited*, *Phys. Rev. D* **105**, 083002 (2022).

- [69] S. Vagnozzi, C. Bambi and L. Visinelli, *Concerns regarding the use of black hole shadows as standard rulers*, *Class. Quantum Grav.* **37**, 087001 (2020).
- [70] K. Jusufi et al., *Black hole surrounded by a dark matter halo in the M87 galactic center and its identification with shadow images*, *Phys. Rev. D* **100**, 044012 (2019).
- [71] S. Vagnozzi et al., *Horizon-scale tests of gravity theories and fundamental physics from the Event Horizon Telescope image of Sagittarius A**, *Class. Quantum Grav.* **40**, 165007 (2023).
- [72] K. Jusufi, *Quasinormal Modes of Black Holes Surrounded by Dark Matter and Their Connection with the Shadow Radius*, *Phys. Rev. D* **101**, 084055 (2020).
- [73] E. Berti, V. Cardoso, and C. M. Will, *On gravitational-wave spectroscopy of massive black holes with the space interferometer LISA*, *Phys. Rev. D* **73**, 064030 (2006).
- [74] G. Franciolini, L. Hui, R. Penco, L. Santoni and E. Trinchirini, *Effective Field Theory of Black Hole Quasinormal Modes in Scalar-Tensor Theories*, *JHEP* **02**, 127 (2019).
- [75] A. Ishibashi and H. Kodama, *Stability of higher dimensional Schwarzschild black holes*, *Prog. Theor. Phys* **110**, 901 (2003).
- [76] D. J. Gogoi and U. D. Goswami, *Quasinormal Modes and Hawking Radiation Sparsity of GUP corrected Black Holes in Bumblebee Gravity with Topological Defects*, *JCAP* **06**, 029 (2022).
- [77] R. A. Konoplya, *Quasinormal behavior of the D-dimensional schwarzschild black hole and the higher order WKB approach*, *Phys. Rev. D* **68**, 024018 (2003).
- [78] X. Zhang, M. Wang and J. Jing, *Quasinormal modes and late time tails of perturbation fields on a schwarzschild-like black hole with a global monopole in the einstein-bumblebee theory*, *Sci. China Phys. Mech. Astron.* **66** 100411 (2023).
- [79] R. A. Konoplya, A. Zhidenko and A. F. Zihhailo, *Higher order WKB formula for quasinormal modes and grey-body factors: recipes for quick and accurate calculations*, *Class. Quantum Grav.* **36**, 155002 (2019).
- [80] R. Karmakar and U. D. Goswami, *Quasinormal modes, temperatures and greybody factors of black holes in a generalized Rastall gravity theory*, *Phys. Scr.* **99**, 055003 (2024).
- [81] S. W. Hawking, *Particle creation by black holes*, *Commun. Math.* **43**, 199 (1975).
- [82] S. W. Hawking, D.N. Page, *Thermodynamics of black holes in anti-de Sitter space*, *Commun. Math.* **87**, 577 (1983).
- [83] J. M. Bardeen, B. Carter, S. W. Hawking, *The four laws of black hole mechanics*, *Commun. Math.* **31**, 161 (1973).
- [84] M. A. Anacleto, F. A. Brito, J. A. V. Campos and E. Passos, *Quantum-corrected scattering and absorption of a Schwarzschild black hole with GUP*, *Phys. Lett. B* **810**, 135830 (2020).
- [85] M. A. Anacleto, F. A. Brito, S. J. S. Ferreira and E. Passos, *Absorption and scattering of a black hole with a global monopole in $f(R)$ gravity*, *Phys. Lett. B* **788**, 231-237 (2019).
- [86] H. Su and C. -Y. Long, *Thermodynamics of the black holes under the extended generalized uncertainty principle with linear terms*, *Commun. Theor. Phys.* **74**, 055401 (2022).
- [87] J. Ji-liang, *Thermodynamics of the black holes under the extended generalized uncertainty principle with linear terms*, *Chinese Physics Letters* **14**, 81 (1997).
- [88] R. T. Hough, A. Abebe and S. E. S. Ferreira, *Viability tests of $f(R)$ -gravity models with Supernovae Type IA data*, *EPJC* **80**, 787 (2020).
- [89] M. Martinelli and A. Melchiorri, *Cosmological constraints on the Hu-Sawicki modified gravity scenerio*, *Phys. Rev. D* **79**, 123516 (2009).
- [90] J. Q. Guo, *SOLAR SYSTEM TESTS OF $f(R)$ GRAVITY*, *IJMPD* **23**, 1450036 (2014).
- [91] S. Nojiri, S. D. Odinstov and V. K. Oikonomou, *Modified gravity theories on a nutshell: Inflation, bounce and late-time evolution*, *Physics Reports* **692**, 1-104 (2017).
- [92] V. F. Cardone, S. Camera and A. Diaferio, *An updated analysis of two classes of $f(R)$ theories of gravity*, *JCAP* **2012**, 030 (2012).
- [93] M. Park, *Can Hawking temperature be negative*, *Phys. Lett. B* **663**, 259-264 (2008).
- [94] S. Dey and S. Chakrabarty, *A note on electromagnetic and gravitational perturbations of the Bardeen de Sitter black hole: quasinormal modes and greybody factors*, *EPJC* **79**, 504 (2019).
- [95] T. Johannsen et al., *Testing General Relativity with the Shadow Size of SGR A**, *Phys. Rev. Lett.* **116**, 031101 (2016).
- [96] D. Psaltis, *Testing General Relativity with the Event Horizon Telescope*, *Gen. Relativ. Gravit.* **51**, 137 (2019).
- [97] P. Kocherlakota et al., *Constraints on black-hole charges with the 2017 EHT observations of M87**, *Phys. Rev. D* **103**, 104047 (2021).